Downloaded from http://sp.lyellcollection.org/ by guest on March 10, 2015

New insights into the Andean crustal structure between 32° and 34°S from GOCE satellite gravity data and EGM2008 model

O. ALVAREZ[1,2]*, M. E. GIMENEZ[1,2], M. P. MARTINEZ[1,2], F. LINCEKLINGER[1,2] & C. BRAITENBERG[3]

[1]*Instituto Geofísico y Sismológico Ing. Volponi, Universidad Nacional de San Juan, Ruta 12, Km 17, CP 5407, San Juan, Argentina*

[2]*Consejo Nacional de Investigaciones Cientificas y Tecnicas, CONICET, Argentina*

[3]*Dipartimento di Geoscienze, Universita di Trieste, Via Weiss 1, 34100 Trieste, Italy*

**Corresponding author (e-mail: orlando_a_p@yahoo.com.ar)*

Abstract: The subduction of the Nazca oceanic plate under the South American plate in the south-central Andes region is characterized by the oblique collision of the Juan Fernandez Ridge against the continental margin. The upper plate is characterized by a broken foreland, a thrust-and-fold belt and eastward migration of the volcanic arc promoted by the flattening of the slab. Topographic load, thermal state and plate rheology determine the isostatic state of the continental plate. We calculated the vertical gravity gradient from GOCE satellite data in order to delineate the main tectonic features related to density variations resulting from internal and external loads. Then, using the Bouguer anomaly, we calculated the crust–mantle discontinuity and the elastic thickness in the frame of the isostatic lithospheric flexure model applying the convolution method approach. The results obtained show substantial variations in the structure of the continental lithosphere related to variations in the subduction angle of the Nazca plate. These variations are reflected in the varying Moho depths and in the plate rigidity, presenting a distinct behaviour in the southern zone, where the oceanic plate subducts with an approximate 'normal' angle with respect to the northern zone of the study area where the flat slab occurs.

The south-central Andes region is characterized by the oblique subduction of the Nazca plate beneath the South American plate. The processes associated with the subduction of the oceanic slab beneath the continental plate, such as flattening, shortening, volcanism and heating, gave rise to the Andes mountains uplift. The shallowing of the Nazca plate in the southern part of the Pampean flat subduction zone has been connected to the collision of the Juan Fernández ridge (JFR) and is based on its potential subducted geometry inferred from hot-spot trajectories conserved on the western Pacific (Yañez *et al.* 2001; Kay & Coira 2009). Deformation of the overriding plate margin under the flat slab region has been associated with the subduction of this elevated oceanic feature (Yañez *et al.* 2001; Yañez & Cembrano 2004; among others). The flat slab can be tracked beneath the continent 500 km from the trench (Sacks 1983; McGeary *et al.* 1985). This segment is associated with vast continental regions elevated above 4000 m and a wide deformational zone that extends beyond 700 km east of the trench.

Gravity field gradients obtained from global gravity field models and from satellite-only data represent an innovative tool for regional gravity modelling. This becomes more meaningful in regions where terrestrial data are sparse or unavailable. Improvements are significant where geological structures are concealed by sediments (Braitenberg *et al.* 2011a) or in mountainous areas (Alvarez *et al.* 2012) where terrestrial access is difficult, and also to overcome problems related to non-unified height measurements from different terrestrial campaigns (Reguzzoni & Sampietro 2010; Gatti *et al.* 2013). Derivatives of the gravity field such as the gravity anomaly (*Ga*) and the vertical gravity gradient (*Tzz*) highlight equivalent geological features related to density differences in a different and complementary way, and are very useful for geological mapping. The vertical gravity gradient is appropriate for detecting mass heterogeneities located in the upper crust where high- and low-density rocks are faced.

The flexural rigidity of the crust is a measure of the lithospheric strength (thickness and viscosity), which in turn depends strongly on lithospheric thermal state and composition (i.e. rheological properties; Lowry *et al.* 2000). The flexural rigidity can be interpreted in terms of the elastic thickness (*Te*) by making some assumptions regarding Poisson's ratio and Young's modulus. The spatial distribution of *Te* is useful to understand the processes related to the isostatic state and deformation of the upper crust, its variation can be explained by temperature distribution and a change of the Young's modulus.

From: Sepúlveda, S. A., Giambiagi, L. B., Moreiras, S. M., Pinto, L., Tunik, M., Hoke, G. D. & Farías, M. (eds) 2015. *Geodynamic Processes in the Andes of Central Chile and Argentina*. Geological Society, London, Special Publications, **399**, 183–202. First published online February 6, 2014, http://dx.doi.org/10.1144/SP399.3
© 2015 The Geological Society of London. For permissions: http://www.geolsoc.org.uk/permissions.
Publishing disclaimer: www.geolsoc.org.uk/pub_ethics

Downloaded from http://sp.lyellcollection.org/ by guest on March 10, 2015

The value of the *Te* is equivalent to the thickness of a corresponding plate with a constant Young's modulus (Wienecke 2006). The base of the mechanical lithosphere for oceanic areas is marked by the approximate depth of the isotherm of 600 °C and presents a good correspondence with the estimated *Te* values. For the continental lithosphere, the relation between specific geological and physical boundaries and the results of *Te* is not so evident (Watts 2001; Wienecke 2006). Different authors (e.g. Goetze & Evans 1979; Lyon-Caen & Molnar 1983; Burov & Diament 1995; Hackney *et al.* 2006) defined a dependence between *Te* and the composition and geometry of the plate, external forces and thermal structure.

In the present study, we examine the interplay between the subduction of the JFR, the subducting Nazca plate and the deformation in the overriding plate on the basis of gravity field modelling. In order to improve the tectonic knowledge of the area under study, our aim is to analyse the geological structure of the crust through gravimetric satellite data. To achieve this goal the new data of the satellite GOCE (Floberghagen *et al.* 2011; Pail *et al.* 2011) was used to calculate the vertical gravity gradient for the south-central Andes area. The same calculation was performed using the global gravity field model EGM2008 (Pavlis *et al.* 2008, 2012), which has higher spatial resolution. Both were corrected for the topographic effect, in a spherical approximation, by using a one arc-minute global relief model of the Earth's surface that integrates land topography and ocean bathymetry (Amante & Eakins 2009). By inverse calculation of the Bouguer anomaly from GOCE data (http://icgem.gfz-potsdam.de/ICGEM/) we obtained the crustal–mantle discontinuity. We later obtained *Te* by flexural modelling. Results were mapped and compared to a schematic geological map of the south-central Andes region, which includes the main geological features with regional dimensions, possibly associated with crustal density variations.

Tectonic setting

The central Chilean margin is marked by the subduction of the JFR (Fig. 1), a hot spot chain formed by intraplate volcanism *c.* 900 km west of the trench, which first collided with the Chilean margin in the north (*c.* 20°) at *c.* 22 Ma, and then moved progressively southwards to the current collision point located at *c.* 32–33°S (Yañez *et al.* 2001). The seamounts are aligned in a chain that trends *c.* 85°E, but changes its strike to a NE direction when approaching the trench (Yañez *et al.* 2001). The collision of the JFR affects the tectonic margin, producing erosion, extensive deformation (von Huene *et al.* 1997) and local uplift where it collides with the continent affecting the entire continental slope (Ranero *et al.* 2006). The subducting plate descends with a maximum dip of 30° from the trench to a depth of *c.* 100–120 km and then flattens underneath the overriding lithosphere for

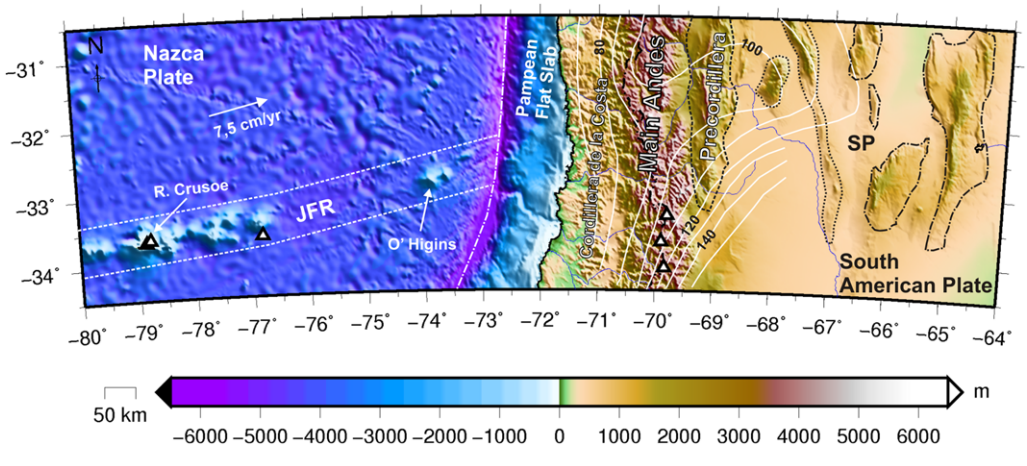

Fig. 1. Shaded DEM of the southern-central Andes region. The JFR is indicated (white dotted line) colliding against the Chilean trench. Robinson Crusoe Island and the O'Higgins seamount are indicated in the figure. The trench is outlined with white dotted and dashed lines. The Precordillera is depicted by a black dashed line, Western Sierras Pampeanas by a black dotted line, and Eastern Sierras Pampeanas by a black dotted and dashed line. These mountain systems were related to the development of the flat slab in the last 17 Ma. A volcanic arc gap is associated with the shallowing of the subducted Nazca plate north of 33°S. SP, Sierras Pampeanas. Triangles indicate the current position of the active volcanic arc (Siebert & Simkin 2002). White solid lines indicate contours of the subducting slab in the Pampean flat-slab zone (Anderson *et al.* 2007). Nazca–South American plates' convergence rate and azimuth are from DeMets *et al.* (2010).

Downloaded from http://sp.lyellcollection.org/ by guest on March 10, 2015

several hundreds of kilometres (*c.* 300 km, Cahill & Isacks 1992; Gutscher *et al.* 2000; Anderson *et al.* 2007) before sinking into the upper-mantle asthenosphere. The asthenospheric wedge is repelled as far as 600 km away from the trench (Brooker *et al.* 2004; Martinod *et al.* 2010).

The southern limit of the Pampean flat-slab segment has been extensively analysed (Jordan *et al.* 1983*a*, *b*; Jordan & Allmendinger 1986; Cahill & Isacks 1992; Anderson *et al.* 2007; among others). Several studies based on hypocentre datasets indicate that the shallowest portion of the flat slab is associated with the inferred location of the subducting JFR at 31°S and that the slab deepens both to the south and north of this region. The gross interpreted structure of the Wadati–Benioff zone of Cahill & Isacks (1992) suggests that the shallowest portion of the slab is spatially correlated with the JFR. Anderson *et al.* (2007) have proposed that the subducting slab geometry is consistent with a buoyant ridge hypothesis for slab-flattening.

The Central Chilean flat-slab segment is expressed superficially by a volcanic gap between 28°S and 32°S, a deformed and faulted foreland zone (Fig. 1) and an expanded Neogene to Quaternary arc volcanism that reached the Sierras Pampeanas (Stauder 1973; Barazangui & Isacks 1976, 1979; Pilger 1981; Jordan *et al.* 1983*a*, *b*; Smalley & Isacks 1987; Kay *et al.* 1988, 1991; Allmendinger *et al.* 1990; Ramos *et al.* 1991, 2002; Cahill & Isacks 1992; Kay & Abbruzzi 1996; Yañez *et al.* 2001). Multiple authors (Allmendinger *et al.* 1997; Kay *et al.* 1999; Gutscher 2000; Kay & Mpodozis 2002; Ramos *et al.* 2002) have linked the eastward expansion and subsequent extinction of the Miocene to Quaternary volcanic arc and contemporary migration of the compressive strain towards the foreland with the gradual flattening of the subducted slab produced from *c.* 15 Ma. The associated change in the thermal structure and consequent shallow fragile–ductile transitions (James & Sacks 1999; Ramos & Folguera 2009) led to the uplift of the Precordillera expressed by a thin-skinned fold and thrust belt and the thick-skinned Sierras Pampeanas, a set of Laramide-style crystalline basement blocks uplifted during the shallowing of the slab from the late Miocene (Fig. 1) (Ramos *et al.* 2002; Kay & Coira 2009).

Global gravity field models

Global Earth gravity field models like EGM2008 (Pavlis *et al.* 2008, 2012) that combine satellite and terrestrial data present a higher spatial resolution (e.g. $N = 2159/\lambda = 19$ km, for EGM2008) than models obtained from satellite-only data (e.g. the preliminary model derived from data of the GOCE mission (Pail *et al.* 2011) with $N = 250/\lambda = 160$ km). The relation between the degree/order of the spherical harmonic development and the spatial resolution is given by $\lambda_{\min} \approx 2\pi R/N_{\max}$ (Barthelmes 2009), where R is Earth's radius and $N_{\max}$ is the maximum degree and order of the expansion. The GOCE model used in this work was obtained from pure satellite GOCE data (e.g. Pail *et al.* 2011; GO_CONS_GCF_2_TIM_R3, http://icgem.gfz-potsdam.de/ICGEM/). The TIM (Time Wise Model) solution is a GOCE-only solution in a rigorous sense as no external gravity field information is used (neither as reference model, nor for constraining the solution). The TIM models have been externally validated by independent GPS/levelling observations for Germany (875 stations) and Japan (873). Results indicate that the lasts pure GOCE-model TIM performs significantly better than EGM2008, even though the latter also contains terrestrial gravity data (see GO_CONS_GCF_2_TIM_xx datasheets, http://icgem.gfz-potsdam.de/ICGEM/). Thus, the GOCE-only gravitational model is useful to evaluate the quality of the terrestrial data entering the EGM2008 by a comparison analysis up to degree $N = 250$ (for degrees greater than $N = 120$, EGM2008 relies entirely on terrestrial data; see Appendix I). Therefore GOCE is a remarkably important independent quality assessment tool for EGM2008. In a recent paper, Braitenberg *et al.* (2011*b*) showed in detail how errors at high degree enter the error of a downscaled EGM2008.

We utilized the convolution approach (Braitenberg *et al.* 2002) to calculate the flexural strength. This method requires the gravity field data on a much smaller scale (on the order of 100 km length) than when using spectral methods (Wienecke 2006). Only the topography must be known over an extensive scale, which depends on the *Te* and therefore the radius of convolution, as explained by Wienecke (2006). The statistical analyses presented (Appendix I) show that the EGM2008 model present errors with respect to the satellite-only model of GOCE, especially in the Andes region. Based on this, we used the satellite-only model of GOCE for calculation of the different quantities derived from the gravity field (e.g. Moho, *Te*, Bouguer, *Tzz*), as it gives greater accuracy. Despite this, the higher spatial resolution of the EGM2008 model was exploited to find the main tectonic features in the *Tzz* map, which then was compared with the *Tzz* map obtained from GOCE (as made in Alvarez *et al.* 2012).

Flexural strength

When calculating the flexural strength of the lithosphere using spectral methods (coherence and

Downloaded from http://sp.lyellcollection.org/ by guest on March 10, 2015

admittance) a large spatial window is required over the study area and the method becomes unstable if the input topography is smooth. Both methods require an averaging process, so the variation in rigidity may be retrieved only to a limited extent (Wienecke 2006). For this reason, these techniques have been questioned when applied to the continental lithosphere. The convolution approach (Braitenberg *et al.* 2002) and the use of a newly derived analytical solution for the fourth-order differential equation that describes the flexure of a thin plate, a concept introduced by Vening-Meinesz in 1939, allow these problems to be overcome (to calculate analytically the deflection of a thin plate for any irregular shape of topography; see Wienecke (2006, and references therein) for a more detailed discussion). This method calculates the flexure parameters by the best fit of the observed crust–mantle interface (e.g. Moho by gravity inversion) and a crust–mantle interface computed with a flexure model. The gravity inversion method and the convolution approach have been tested extensively in synthetic models and in different geographical areas (Braitenberg *et al.* 1997, 2002; Braitenberg & Drigo 1997; Zadro & Braitenberg 1997; Braitenberg & Zadro 1999; Ebbing *et al.* 2001; Wienecke 2002, 2006; Pérez-Gussinyé *et al.* 2004; Bratfisch *et al.* 2010; Steffen *et al.* 2011; Ferraccioli *et al.* 2011).

Methodology

To accomplish the inverse modelling of flexural rigidity we used the Lithoflex software package (www.lithoflex.org) (Braitenberg *et al.* 2007; Wienecke *et al.* 2007). This tool fulfils a series of different functions that are concerned with studying the gravity field as well as the isostatic state, and combines forward and inverse calculation for gravity and flexural rigidity. The evaluation method used in these calculations allows a relatively high spatial resolution, superior to spectral methods (see Braitenberg *et al.* (2007) for more detail). Isostatic modelling adopts the isostatic thin plate flexure model (e.g. Watts 2001). To perform isostatic calculations, that is, to estimate the elastic properties of the plate for a known load, a crustal load and the crust–mantle interface need to be used as a reference surface (Wienecke 2006). The load acting on the crust is provided as the combination of the overlying topography and a density model (Braitenberg *et al.* 2007). A density variation within the crust represents a variation in the load and must be reflected in the isostatic response (Ebbing *et al.* 2007). The topographic load was calculated using topo/bathymetry data from ETOPO1 (Amante & Eakins 2009), while the densities used for calculation were 1.03 g cm^{-3} for water and 2.8 g cm^{-3} for the crust.

The undulating boundary or discontinuity corresponding to the Moho was calculated from observed gravity data by gravity inversion. The Bouguer anomaly field used for the gravity inverse calculations was obtained from the Calculation Service of the International Centre for Global Earth Models (ICGEM, http://icgem.gfz-potsdam.de). The Bouguer anomaly was calculated using the GOCE satellite data (Pail *et al.* 2011) up to degree/order $N = 250$. Long-wavelength information of the gravity field mainly corresponds to the crust–mantle density contrast, but sedimentary basins can also produce a long-wavelength signal, thus influencing the correct gravity crust–mantle interface estimation by the gravity inversion process (Wienecke 2006). Therefore, the gravity effect of sediments was calculated in order to reduce the gravity data.

The forward calculation of the gravity effect for the sediment package (Fig. 2) was calculated taking into account a linear variation of density with depth. To perform this calculation we defined a two-layer reference model of the continental crust with the following densities: upper crustal density, 2.7 g cm^{-3}; lower crustal density, 2.9 g cm^{-3}. The relation density/depth was defined using a linear variation (see Braitenberg *et al.* 2007). To perform this operation we used the bathymetry from ETOPO1 (Amante & Eakins 2009) and off-shore sediment thickness from Divins (2003). On-shore basins were modelled using depths to top basement from gravimetric studies and the seismic lines of Yacimientos Petroliferos Fiscales (YPF), Texaco, Repsol YPF, YPF S.A. and OIL M&S, and from Kokogian *et al.* (1993), Milana & Alcober (1994), Fernandez Seveso & Tankard (1995), Miranda & Robles (2002), Rosello *et al.* (2005) and Barredo *et al.* (2008). The correction amounts were up to −40 mGal for the main onshore basins and up to a few mGal for oceanic sediments, reaching their maximum over the Chilean trench.

From this reduced Bouguer anomaly (Fig. 3) we estimated the gravimetric crust–mantle discontinuity (Fig. 4) by gravity inversion. This method uses an iterative algorithm that alternates downward continuation with direct forward modelling (Braitenberg & Zadro 1999) and is somewhat analogous to the Oldenburg–Parker inversion approach (Parker 1972; Oldenburg 1974; see Braitenberg *et al.* (2007) for a detailed explanation). This method requires two input parameters: density contrast and reference depth. The density contrast between crust and mantle is unknown and has to be assumed as a constant value. Standard parameters such as normal crust thickness $Tn = 35$ km, and a crust–mantle density contrast of −0.4 g cm^{-3} were used.

Downloaded from http://sp.lyellcollection.org/ by guest on March 10, 2015

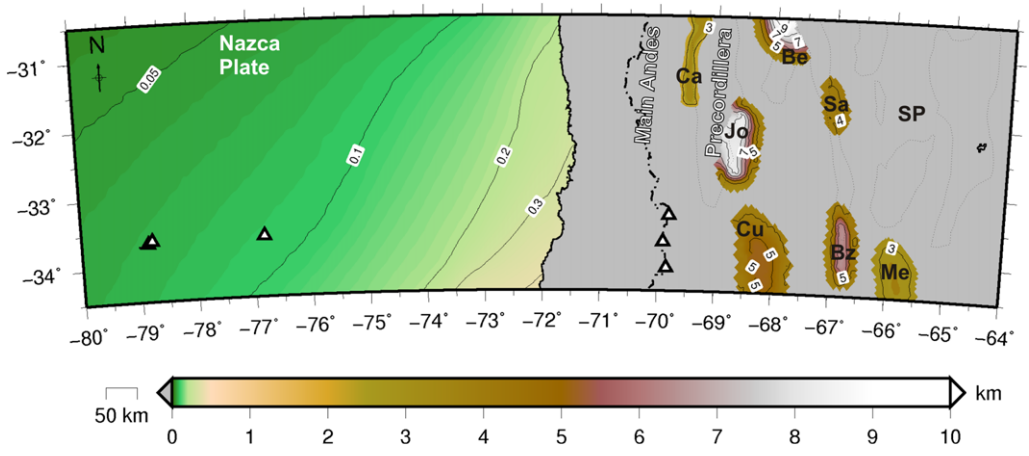

Fig. 2. Sediment thickness used to reduce the gravity data. Offshore sediment thickness is from Divins (2003). The basins over the South American plate were approximated using gravity databases and basement depths from seismic lines (YPF S.A. unpublished report)

For the inverse flexure calculation, the crustal load (obtained from topo/bathymetry data and the density model) and the Moho undulations (obtained by inversion of the reduced Bouguer anomaly) were utilized. The flexural rigidity is inverted in order to match the known loads with the known crustal thickness model (i.e. to model the gravity Moho in terms of an isostatic model). The elastic thickness was allowed to vary in the range $1 < Te < 50$ km and was iteratively estimated over moving windows of size 80 km × 80 km. The model parameters are given in Table 1, where the adopted densities are standard values already used by Introcaso *et al.* (2000), Gimenez *et al.* (2000), Miranda & Robles (2002) and Gimenez *et al.* (2009).

The difference between the Moho from gravity inversion and the flexure Moho is the residual Moho (gravity Moho minus flexure Moho) (Fig. 5). The Moho undulations obtained from gravity inversion agree with the CMI undulations expected for the flexural model, *c.* 90% within 3 km of difference (Fig. 6). Positive values of the residual Moho indicate that the gravity Moho is shallower than the flexure Moho, which is the case when high-density rocks are present in the crust,

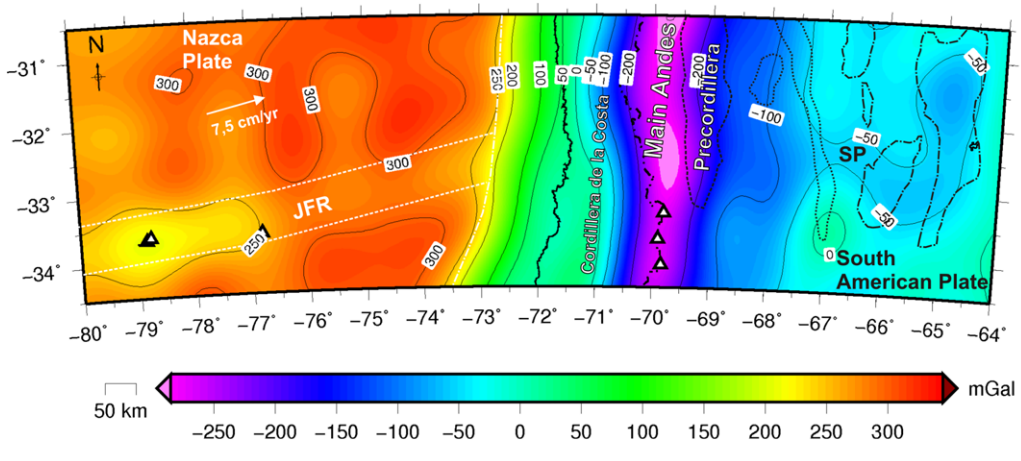

Fig. 3. Sediment corrected Bouguer anomaly field used for the inversion of the crust–mantle interface. The Bouguer anomaly was obtained from GOCE up to degree and order 250 (Pail *et al.* 2011). The JFR can be tracked by a well-defined gravity signal. The main Andes presents a low gravity signal representative of the Andean root.

Downloaded from http://sp.lyellcollection.org/ by guest on March 10, 2015

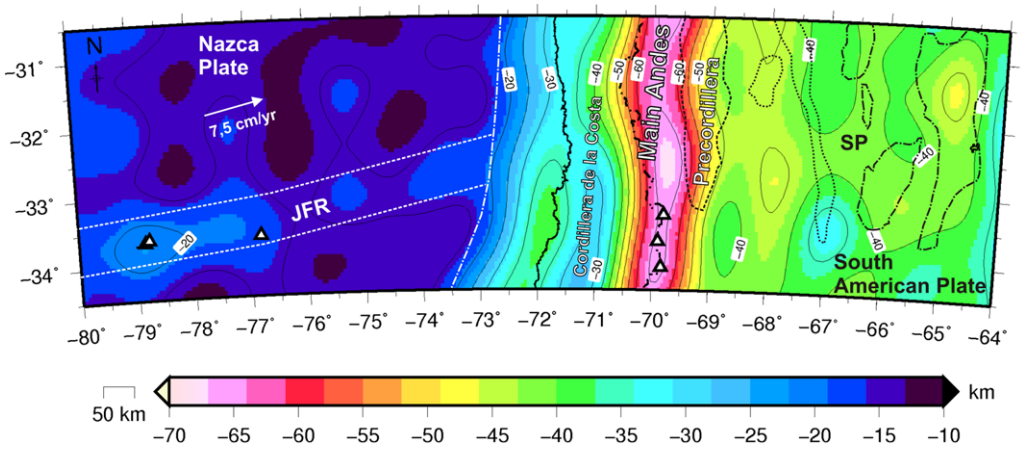

Fig. 4. Moho undulations obtained by inversion of the sediment corrected Bouguer anomaly. The Moho depths indicate the existence of an over-thickened oceanic crust in the JFR path. East of the trench, the contours exhibit a distinct behaviour north and south of the ridge. The Andean root presents depths of more than −60 km.

as in the Cordillera de la Costa (Figs 7 & 8). Correction of the gravity and load effect of the sediments at sedimentary basins allows gravity Moho to comply with load changes: once the negative effect on the Bouguer from the sediments is removed, the Moho from gravity inversion will be shallower and will follow the flexure Moho. When at sedimentary basins there are positive values of residual Moho this is an indication of increased crustal densities below the basin. Negative values of the residual Moho in the Main Andes indicate that the gravity Moho is deeper than the flexure Moho, as the Bouguer anomaly is strongly influenced by the negative effect of the Andean root. The flexural model used in this work is a simplification and would be influenced by the stress of the downgoing plate. Thus, the *Te* solutions along the active subduction margin could be distorted (as explained by Braitenberg *et al.* 2006). Gimenez *et al.* (2000) found that the effect of the flattened Nazca plate has a positive gravimetric effect (max. of 100 mGal) in the flat-slab region with very long wavelengths. This effect over the Bouguer anomaly then produces an increase in the Moho depth of *c.* 7–10 km (max.), again with very long wavelengths. Not accounting for this effect in our calculations does not change the conclusions.

Table 1. *Parameters used in the flexural modelling*

Masses above sea-level	ρ_s	2.67 g cm^{-3}
Upper crustal density	ρ_{uc}	2.7 g cm^{-3}
Lower crustal density	ρ_{lc}	2.9 g cm^{-3}
Upper mantle density	ρ_m	3.3 g cm^{-3}
Young modulus	E	10^{11} N m^{-2}
Poisson ratio	Σ	0.25

Vertical gravity gradient *Tzz*

As previously explained, the lithosphere deforms in response to topographic and internal loads. To delineate the geological structures related to density variations at a regional scale, we calculated *Tzz* in terms of the spherical harmonic coefficients up to degree/order $N = 250$ for GOCE (Pail *et al.* 2011) and up to degree/order $N = 2159$ for EGM2008 (Pavlis *et al.* 2008), on a regular grid with a cell size of 0.05°. The need for higher resolution to perform this task justifies the calculation with the EGM2008 model, while considering that some areas exhibit differences with respect to GOCE. For geological mapping, the vertical gravity gradient is ideal, as it highlights the centre of the anomalous mass (Braitenberg *et al.* 2011*a*). This allows unknown geological structures to be revealed that are either concealed by sediments or that have not been mapped previously.

The topographic effect is removed from the potential field derivatives to eliminate the correlation with the topography (see Alvarez *et al.* (2012) for more details). The calculation height is 7000 m to ensure that all values are above the topography, and topographic mass elements are approximated with spherical prisms to take into account the Earth's curvature (Uieda *et al.* 2010). The topographic correction amounts to tens of Eötvös for the vertical gradient and up to a few hundred mGal for gravity and is greatest above the highest topographic elevations and above the lower topographic depressions, as in the Chilean trench.

Downloaded from http://sp.lyellcollection.org/ by guest on March 10, 2015

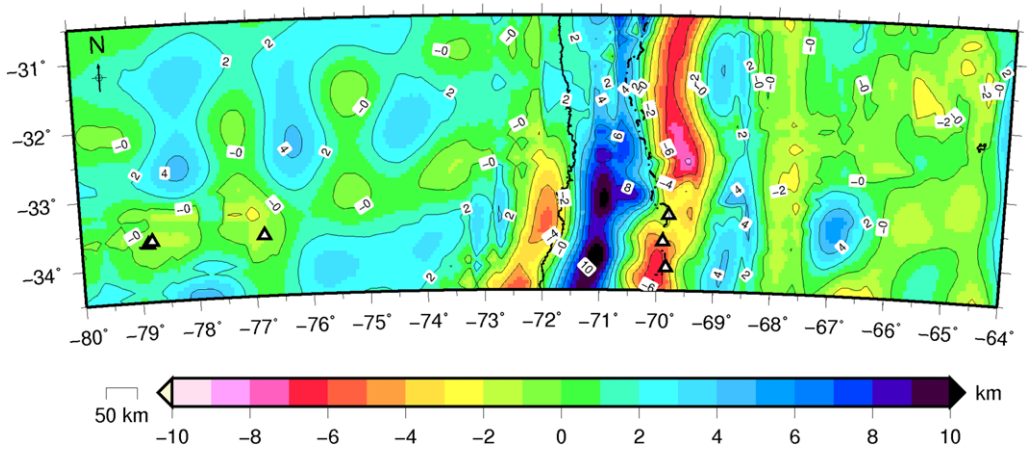

Fig. 5. Residual obtained by subtracting the crust–mantle interface obtained by gravity inversion of the Bouguer anomaly minus the crust–mantle interface obtained from the flexural model.

Results

To perform interpretation and determine the relation of the main geological units in a regional dimension, the *Tzz* and Bouguer anomaly were compared. A comparison of the fields reveals that the locations of the anomalies are well-correlated, but the *Tzz* highlights more detail than the gravity, as explained by Braitenberg *et al.* (2011*a*). We first analysed the *Tzz* obtained with the EGM2008 model as it presents the greatest spatial resolution available to date, taking into account the presence of some differences with respect to the pure satellite GOCE data (see Appendix I). The *Tzz* obtained with GOCE was then analysed and contrasted with the results obtained with EGM2008. This allows us to determine the location and morphology of the geological structures related to density variations in an optimal way, as done by Braitenberg *et al.* (2011*a*) and Alvarez *et al.* (2012).

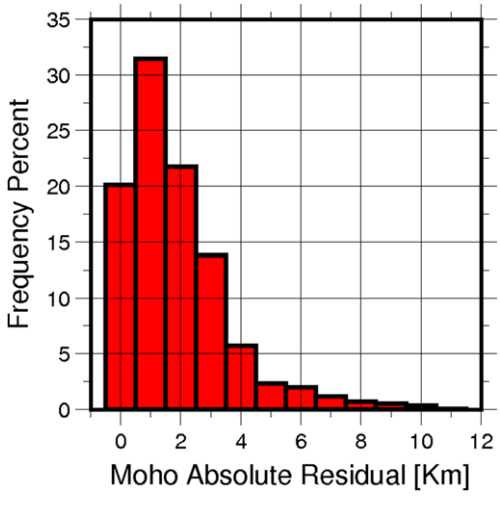

Fig. 6. Histogram of the residual Moho between the crust–mantle interface obtained by gravity inversion and the crust–mantle interface from the flexural model. More than 90% of the error is less than 4 km.

The track of the JFR is delimited by a well-defined gravimetric signal lower than the surrounding plate, reaching its minimum expression over the seamount chain and islands with less than +250 mGal (Fig. 3). The *Tzz* obtained with GOCE (Fig. 8) presents values less than −5 Eötvös in the vicinity of the Robinson Crusoe Island, and increases its values as it approaches the trench. The *Tzz* obtained with EGM2008 (Fig. 7) exhibits different positive anomalies of more than +25 Eötvös, an expression of the numerous small volcanic edifices and hot-spot derived seamounts over the JFR (e.g. the O'Higgins seamount is expressed by a high *Tzz* value). These positive anomalies are not detectable in the GOCE *Tzz* map (Fig. 8) as a consequence of the lower spatial resolution; that is, the high-wavelength character of the GOCE signal does not resolve the high-frequency anomalies.

Seaward of the trench, the flexural bulge of the downgoing Nazca plate is marked by a positive anomaly in the *Tzz* signal greater than +20 Eötvös (Fig. 7). This is not apparent in the *Tzz* obtained with GOCE, although it is also detectable (Fig. 8) by the +15 Eötvös contour, which is segmented by the ridge path. Eastward from the trench to the coastline, the values of the *Tzz* anomaly reflect the differences of the trench sediment infill south and

Downloaded from http://sp.lyellcollection.org/ by guest on March 10, 2015

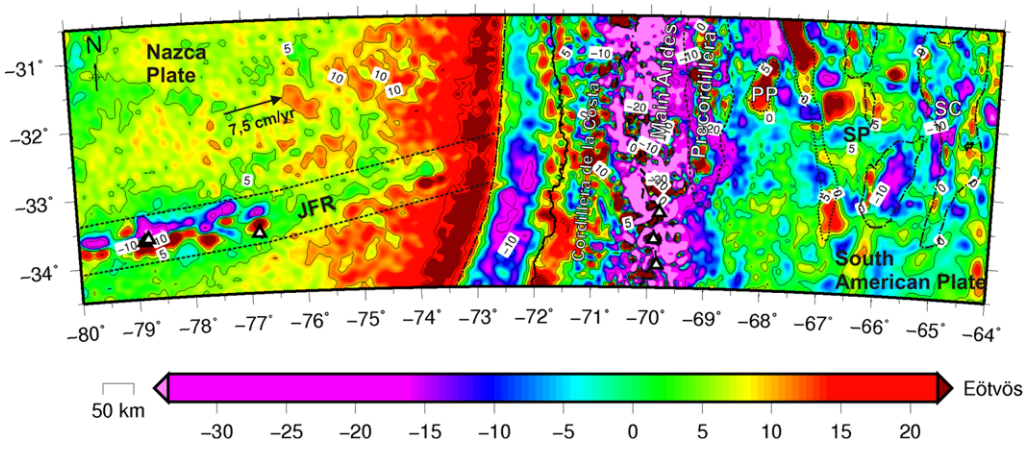

Fig. 7. Map of the vertical gravity gradient (EGM2008 up to degree and order 2159) corrected by topography. The seamounts of the JFR (black dotted line) can be tracked by a high gradient signal. The flexural bulge exhibits a high gradient signal that parallels the Chilean trench (black dotted and dashed line). The main Andes presents a low gradient signal representative of the Andean root. The Precordillera (black dashed line) exhibits high gradient values. Western Sierras Pampeanas is depicted by a black dotted line and Eastern Sierras Pampeanas by a black dotted and dashed line. White triangles indicate the current position of the active volcanic arc (Siebert & Simkin 2002).

north of the collision point of the JFR. To the south, the *Tzz* values are lesser than −10 Eötvös, and to the north the *Tzz* signal increases, indicating the abrupt decease in the sediment infill in this region (Figs 7 & 8).

Inland, the negative gravimetric effect of the Andes Cordillera presents a smaller amplitude in the southern direction, reflecting the lower Andean elevations and the consequent reduction of the Andean root. This can be observed in the Bouguer anomaly, which has smaller values to the north (< −300 mGal) than to the south (Fig. 3), whereas the *Tzz* signal has values of < −30 Eötvös (Fig. 8). The *Tzz* obtained with the model EGM2008 exhibits some positive anomalies higher than +25 Eötvös within this negative response (Fig. 7). West to the

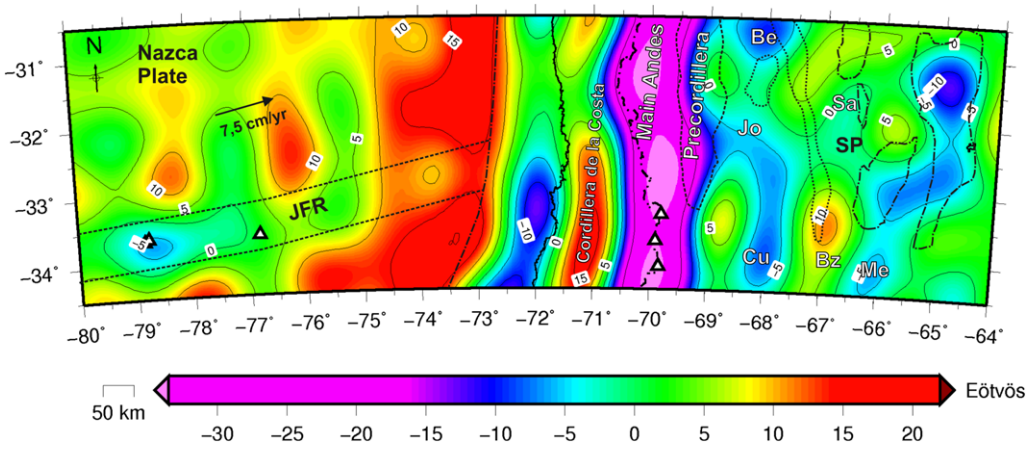

Fig. 8. Map of the vertical gravity gradient (GOCE up to degree and order 250) corrected by topography. The path of the JFR can be tracked by a low gradient signal relative to the surrounding plate. The effect of the Andean root over the gradient signal is notorious. A higher gradient signal is located in the Precordillera and in Western Sierras Pampeanas. Sedimentary basins: Be, Bermejo; Jo, Jocoli; Sa, Salinas; Cu, Cuyana; Bz, Beazley; Me, Mercedes.

Downloaded from http://sp.lyellcollection.org/ by guest on March 10, 2015

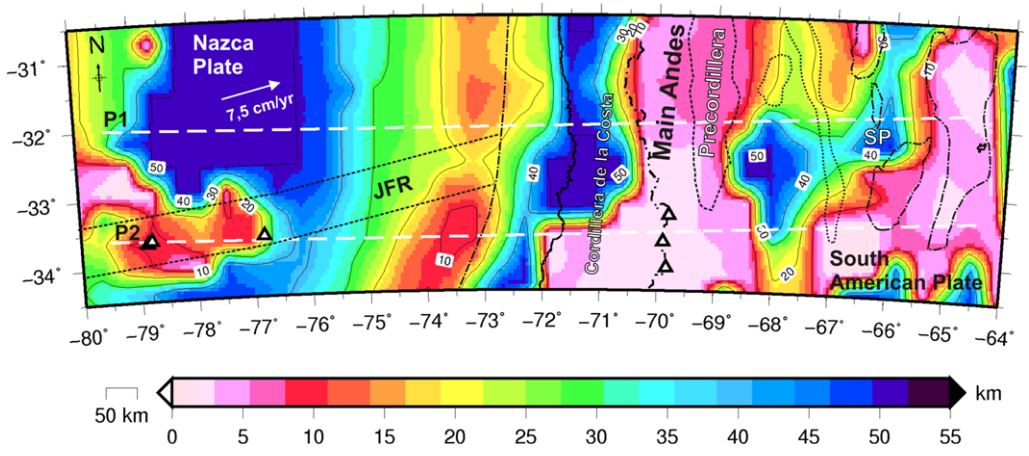

Fig. 9. Elastic thickness values obtained for the region. Note the weakening of the oceanic lithosphere in the ridge path and over the flexural bulge. A region of great rigidity is located in the forearc over the flat-slab region. The compensation to the topographic load of the main Andes is expressed by low *Te* values. To the west of the active volcanic arc, the low *Te* values are the expression of a weakened crust due to heating of the asthenospheric wedge. A more rigid plate is located to the east of the main Andes up to the location of Eastern Sierras Pampeanas.

Main Andes and to the coast line, the Cordillera de la Costa presents a positive gravimetric response and high *Tzz* values.

The positive gravimetric response of the Precordillera within the general negative trend marked by the Andean root is clearly depicted in both *Tzz* maps, with higher resolution over the EGM2008 *Tzz* map (Fig. 7), and is marked by the 0 Eötvös contour in the GOCE *Tzz* map (Fig. 8). The gravity anomaly map presented by Alvarez *et al.* (2012) also exhibits a different response of the Precordillera with respect to the Main Andes, presenting higher values. Other works (Introcaso *et al.* 1992; Gimenez *et al.* 2000, among others) also report a high gravimetric signal for the Precordillera based on terrestrial gravimetric data. These gravimetric highs in the northern Precordillera could be related to denser bodies generated by the fusion of the continental lithosphere through intrusion of asthenospheric magmas (Astini *et al.* 2009; Dahlquist *et al.* 2010).

Sedimentary basins such as Jocoli, Cuyana, Mercedes, Bermejo and Beazley basins exhibit low *Tzz* values, while the Salinas basin exhibits more intermediate values (Fig. 8). North of Beazley Basin we observe a high *Tzz* value greater than +10 Eötvös (Figs 7 & 8). This anomaly was also detected in the Bouguer anomaly map (more than +50 mGal) obtained with GOCE and corresponds to the Quijadas range, the southernmost expression of the Western Sierras Pampeanas (SP).

The Pie de Palo (PP) mountain range, an exposure of Mesoproterozoic crystalline basement and the westernmost expression of the western SP, was identified in the EGM2008 map (Fig. 7) by a high *Tzz* signal of more than +70 Eötvös. This is undetectable with GOCE because its topographic signal has a magnitude on the order of the spatial resolution of the model derived from GOCE. East of PP are the Western SP, which are mainly composed of Ordovician plutonic rocks. These mountains, which form part of the Famatinian arc (Fig. 10b) within the SP, exhibit high *Tzz* values greater than +20 Eötvös (Fig. 7). The easternmost region of the SP is characterized by the Sierras de Cordoba (SC), basement-cored uplifts that present low *Tzz* values because the density of granitic rocks is lower than 2.67 g cm^{-3}.

Once the spatial locations of the main anomalies related to density variations were determined, we analysed their relation with plate strength variations. Figure 12 shows the relation between elastic thickness *Te* (Fig. 9), the gravimetric crust–mantle discontinuity (Fig. 4) obtained from the inversion of the sediment corrected Bouguer anomaly (Fig. 3), and *Tzz* (Fig. 8).

Above the Nazca Oceanic plate, the Moho undulations delineate the track of the JFR, which reaches its maximum depth (*c.* −30 km) over Robinson Crusoe Island (Fig. 4). The *Te* over the seamount chain presents low values (Figs 9 & 10a) indicative of the bending of the oceanic plate in this area (consequence of the topographic load and a young, warm oceanic lithosphere). This is consistent with the Bouguer anomaly (Fig. 3), which presents lower values over the ridge than over the surrounding plate. Previous studies (Wienecke 2006) have also shown a good correlation between lower *Te* values and the occurrence of seamounts, especially in the

Downloaded from http://sp.lyellcollection.org/ by guest on March 10, 2015

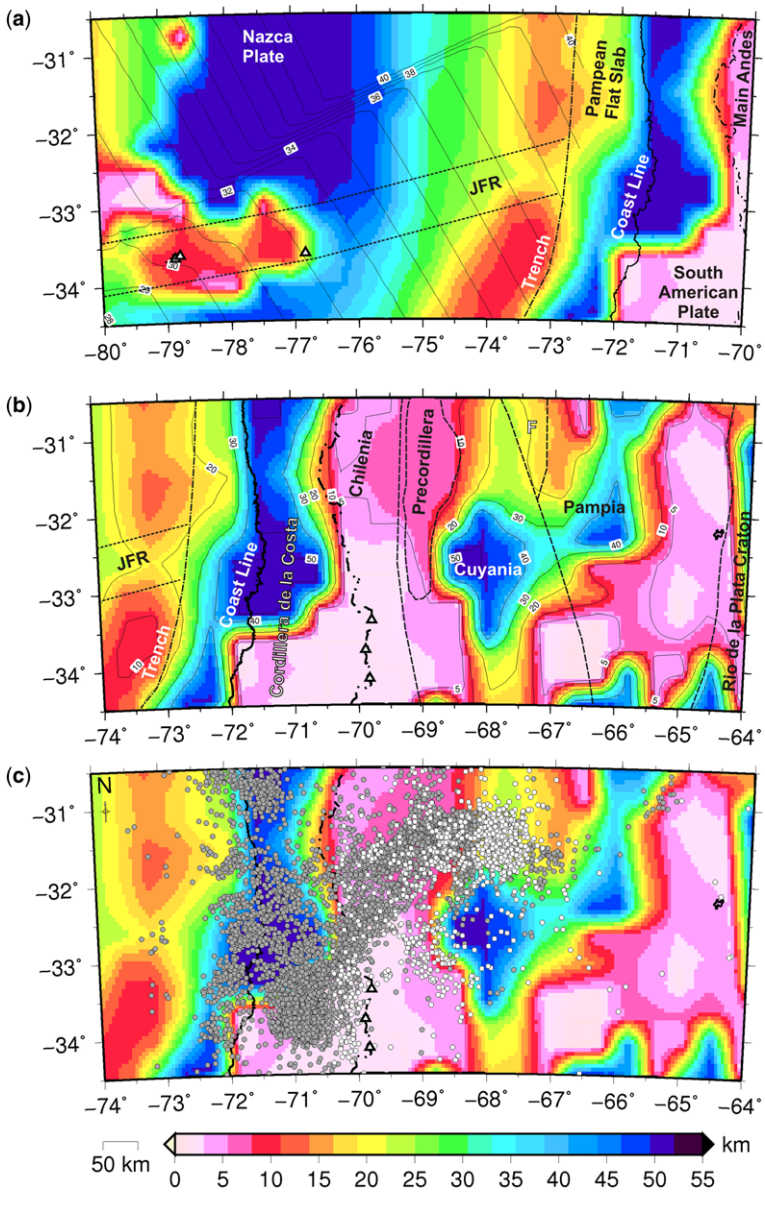

Fig. 10. (**a**) Elastic thickness values obtained for the Nazca plate. Superimposed age plates from Müller *et al.* (2008). (**b**) Elastic thickness values obtained for the South American plate. Superimposed terranes from Ramos (2009) and Ramos *et al.* (2010). F, Famatina. (**c**) Hypocentres of seismicity (EHB Catalog) for crustal earthquakes (white circles) and subducted Nazca plate earthquakes (grey circles).

area of the Sala y Gomez Ridge, Nazca Ridge and Juan Fernandez Ridge. Other work has reported an over-thickened oceanic crust beneath the JFR based on wide-angle seismic data (von Huene *et al.* 1997) and also related negative satellite-derived gravity anomalies to a crustal root indicative of crustal flexure from loading associated with seamounts (Sandwell & Smith 1997).

Towards the trench the Moho undulations, expression of the ridge path, are shallower and the *Te* decreases (to 30 km). An inflexion in the *Te* signal occurs where the ridge path intersects the

Downloaded from http://sp.lyellcollection.org/ by guest on March 10, 2015

bent oceanic plate prior to subduction (Figs 9 & 10a). We obtained higher values of *Te* over the ridge track and smaller values south and north of it over the fore bulge (less than +15 km) where the astenosphere is more superficial. These minimum values of *Te* at the flexural bulge are coincident with high plate curvatures, strong bending moment, fracturing and faulting of the oceanic basement and a reduction in crustal and mantle seismic velocities in this region, as mentioned by Contreras-Reyes & Osses (2010). These authors also reported a reduction in flexural rigidity towards the trench and related this to a weakening of the oceanic lithosphere.

Another factor to consider is the age of the subducting plate. Conductive cooling exerts a primary control over the strength of the oceanic lithosphere (Watts 2001), so its strength is greater where it is cooler and older. A cooler subducted lithosphere may reduce heat from the base of the upper plate (Yañez & Cembrano 2004; Tassara 2005). Before subduction, the Nazca plate ages range from 38 to 42 Ma north of the JFR, while to the south it is younger than 38 Ma (Fig. 10a). These slight differences in age may also contribute to the greater strength estimated in the flexural-bulge region north of the JFR. Note that the flexural bulge presents lower *Te* values south of the JFR where the plate is younger. However, this is not conclusive, as other factors must be taken into account such as the loading history of the plate prior to subduction, as explained by Contreras-Reyes & Osses (2010). The JFR is an important barrier, restraining the transport of sediment along the trench axis separating a heavily sedimented trench to the south from a trench north of 32.5°S that is starved of sediment or contains less than 1 km thickness of turbidites confined to a narrow axial zone (Bangs & Cande 1997, among others). Taking this into account, the lower *Te* values over the fore bulge to the south of the JFR when compared to the north should be a consequence of the combined effect of a younger and warmer lithosphere and to the sediment load.

East to the trench, the *Te* exhibits distinct behaviour north and south of the JFR trend. To the north, in the flat-slab region, the oceanic Moho deepens more gradually than to the south. In the forearc region, the subducting slab reverses its flexural curvature to flatten and travels subhorizontally (see profiles from Anderson *et al.* (2007), Fig. 11). The flattening of the slab repels the asthenospheric wedge far inland, hundreds of kilometres east, generating a conductive cooling of the continent, which is reflected by its increased strength. In this area the *Te* values increase towards the coastline, indicating an increasing rigidity eastwards (Figs 9 & 10b). Previous work has also found high *Te* values over the flat-slab regions (Stewart & Watts 1997; Tassara 2005). Interplate seismicity (Engdahl *et al*. 1998; EHB 2009) is well correlated with high *Te* values in the forearc region (Fig. 10c).

In a previous work, Pérez-Gussinyé *et al.* (2008) proposed that the flat slabs are characterized by high *Te* values, high shear wave velocity, thick thermal lithosphere and low heat flow, indicating that the continental lithosphere is thicker and cooler. The estimated *Te* in this area, where the upper plate and the subducted slab are in contact, can be expected to have contributions from both plates (see Pérez-Gussinyé *et al.* (2008) for a detailed discussion) and the *Te* values without other constraints cannot distinguish if the high flexural rigidity is also reflecting a thicker and stronger continental lithosphere prior to subduction.

To the south of the collision of the JFR, the oceanic plate presents a 'normal' dip angle of *c.* 30° and the active volcanic arc is located roughly above the 110 km isodepth contour of the slab (Fig. 1). Here, the oceanic Moho deepens more rapidly than in the northern zone and exhibits a depth of more than 40 km in the vicinity of the coastline. Anderson *et al.* (2007) obtained *c.* 50 km of depth to Moho from seismicity data. The higher values of *Te* (40 km) east to the trench may be interpreted as upper plate cooling by the underlying slab, which displaces the thermal structure downwards. The opposite occurs at the forearc region where the upper plate and the slab decouple, where melting ascends in the volcanic arc and basal heating by the asthenospheric wedge flow produces advective heating of the upper plate. Thus, low *Te* values estimated in this area reflect a weakened upper plate in the forearc to the south of the ridge collision point (Figs 9 & 10b).

The Moho depths obtained for the main Andes reach more than 66 km over the Andean axis and *Te* values are lower than 5 km (Figs 9 & 10b). Moho depths are consistent with those obtained by Gans *et al.* (2011) (70 km) for the main Cordillera, based on 'receiver functions'. In the backarc, the low gravity anomalies and low *Te* values affect the flexural root of the main Andes. This low *Te* value corresponds to a flexural model where the plate has no strength, the classical Airy model for local compensation. Similar results have been obtained previously by other authors, such as Introcaso *et al.* (1992), who explained that the Andes would be near the isostatic balance. The results are also consistent with other previous work for the Andean region (Stewart & Watts 1997; Tassara & Yañez 2003; Tassara *et al.* 2007; Pérez-Gussinyé *et al.* 2008; Sacek & Ussami 2009).

The Precordillera exhibits a different behaviour from that of the main Andes; the crust–mantle interface is more superficial, and higher values of *Te* are

Downloaded from http://sp.lyellcollection.org/ by guest on March 10, 2015

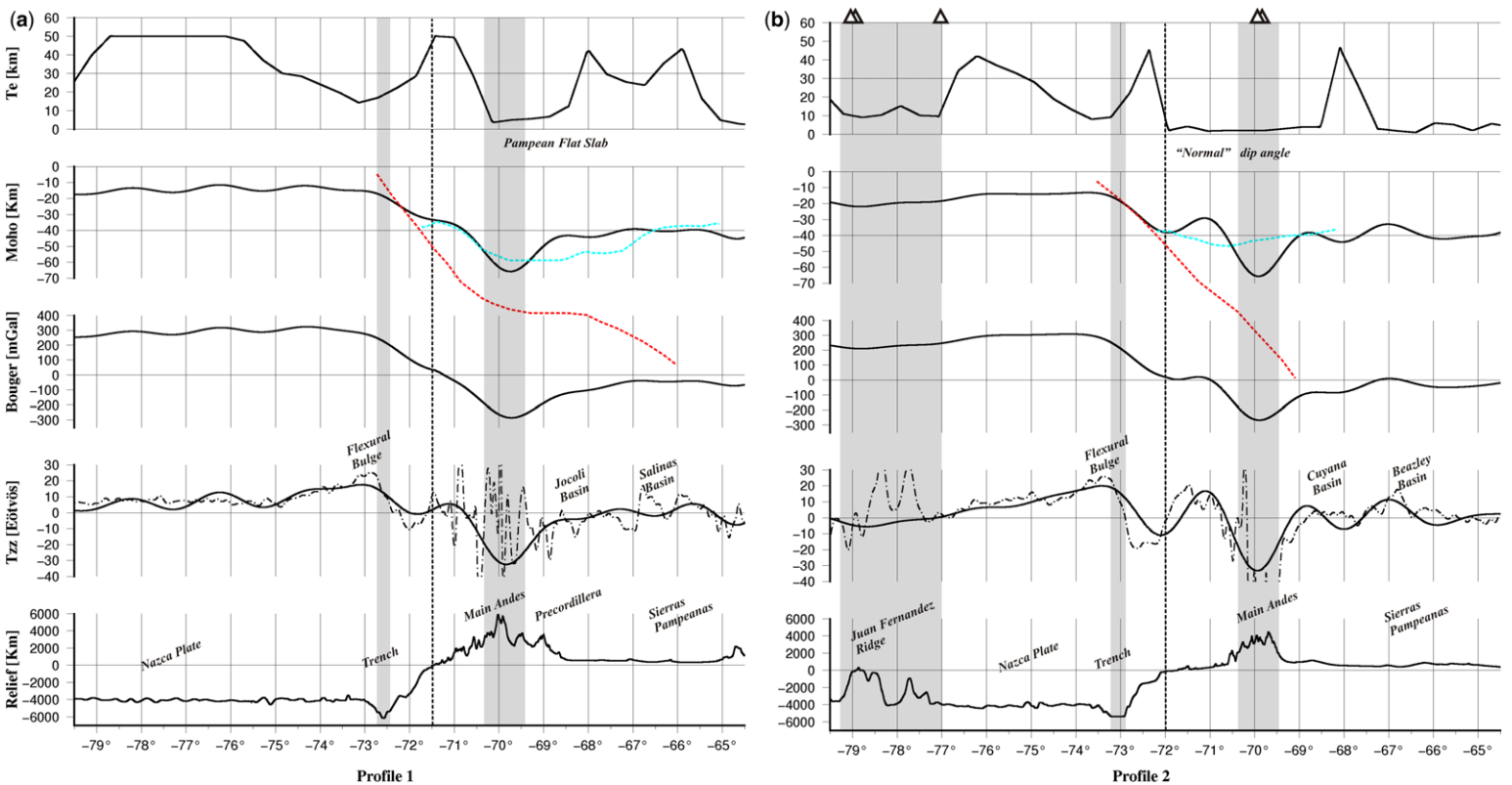

Fig. 11. Profiles comparing the topography corrected vertical gravity gradient, Bouguer anomaly, Moho depths and elastic thickness obtained by GOCE up to $N = 250$, over the northern region. (**a**) Profile 1: grey shaded area depicts the trench and the main Andes. (**b**) Profile 2: grey shaded area depicts the trench, the main Andes and the JFR. Dotted and dashed line indicates *Tzz*-EGM2008 corrected by topography; dashed line indicates the coastline; red dashed line indicates profiles of the Wadati–Benioff zone; blue dashed line indicates Moho depths from Anderson *et al.* (2007).

Downloaded from http://sp.lyellcollection.org/ by guest on March 10, 2015

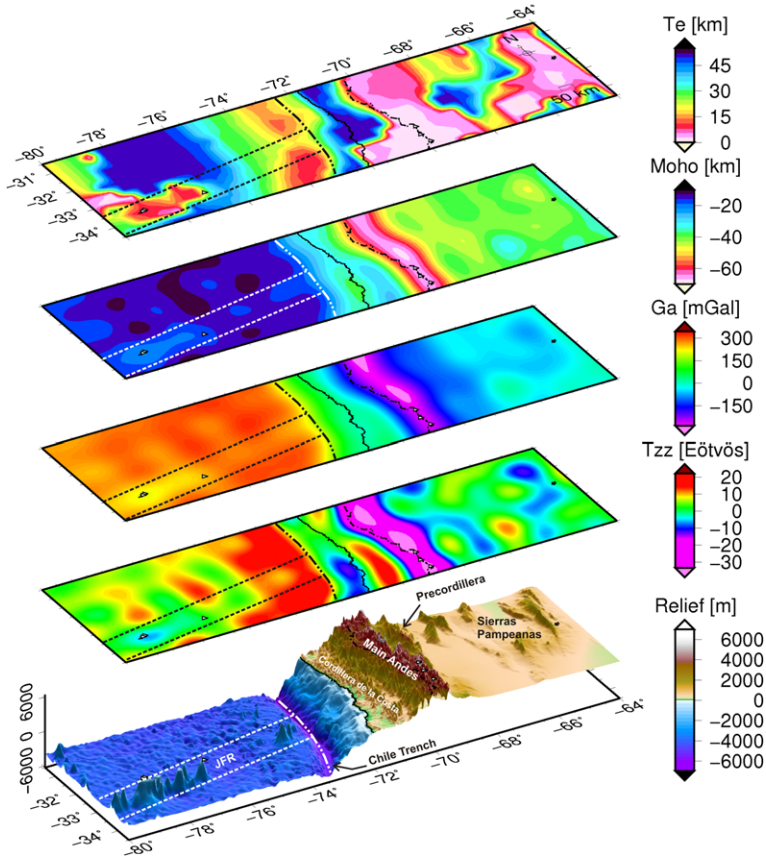

Fig. 12. Relation between the elastic thickness (uppermost and downwards), Moho, Bouguer, vertical gravity gradient and relief. Note the relation between the ridge path, which can be delineated in all signals, and the differences north and south of it in the region east of the trench to the volcanic arc. The effect of the Andean root is also well correlated in all quantities. The high gravity gradient signal obtained in the southernmost region of the Sierras Pampeanas is also observed in the Bouguer anomaly, in the Moho depths and in the elastic thickness, although there is no evident topographic signal in this region.

detected in this area. The Western SP are characterized by more intermediate Moho depths (between 40 and 50 km) and intermediate *Te* values (*c.* 20 km) indicative of a more global compensation (Figs 9 & 10b). Moho depths are consistent with those obtained by Gans *et al.* (2011). In this area the *Tzz* map indicates the presence of high- density bodies (Fig. 7). Weidmann *et al.* (2013) also found high-density areas with high flexural rigidity in the Western SP, based on terrestrial data. This is consistent with the tectonic evolution of these mountains, which were elevated by listric faults and thus do not present a local compensation. Quite the opposite occurs at the southern ending of the Western SP. In this region a low value of *Te* is detected (Figs 9 & 10b), which is well matched with a shallowing of the Moho (Figs 4 & 12). In this area there is no significant topographic expression, but there are high *Tzz* values (Figs 7 & 8) and high Bouguer anomalies (Fig. 3) related to the Sierra de la Quijadas, as previously stated. This low plate rigidity is well correlated with an absence of intraplate seismic activity in the area (Fig. 10c).

The SC are the easternmost expression of the SP and form the eastern border with the Rio de la Plata Craton (Fig. 10b). These mountain ranges are characterized by shallower Moho depths (*c.* 40 km), consistent with previous work (Gans *et al.* 2011). *Te* values indicate low rigidity under these ranges and increasing values to the east where the Rio de la Plata Craton is located (Fig. 10b). The Sierra de San Luis, the southwesternmost expression of the eastern SP, presents *Te* values ranging from 5 km to 30 km, increasing in the northwestern direction. Sedimentary basins such as

Downloaded from http://sp.lyellcollection.org/ by guest on March 10, 2015

Jocoly and Mercedes basins exhibit high rigidity values, while the Bermejo, Cuyana and Salinas basins have more intermediate values.

An approximate correlation between different terranes and plate rigidity was found (Fig. 10b). The Precordillera Terrane exhibits an homogeneous *Te* value of *c.* 7 km. Cuyania presents high rigidity, which is diminished by the asthenopheric wedge to the south. Famatina has intermediate *Te* values. An inflection in the *Te* is observed on the border between the Pampia Terrane and the Rio de la Plata Craton where the values increase indicating more plate rigidity.

Profiles across the region

Two different profiles were traced over the study region in the west–east direction (for location of profiles see Fig. 9). Profile 1 (Fig. 11a) was traced in the northern region at 32°S where the flattening of the slab occurs. Profile 2 (Fig. 11b) was traced at 33.5°S and cut along the JFR to the active volcanic arc.

North of the JFR the *Te* values (Fig. 11a) are more than +50 km, indicating a more rigid part in this area. Tebbens & Cande (1997) proposed that these rigid parts surrounded by areas of lower *Te* values, as well as between the Nazca Ridge and the JFR (see Fig. 9), might indicate the existence of microplates. Towards the trench the plate rigidity decreases, reaching up to +15 km in the flexural bulge, which is well defined by a high *Tzz* signal (Fig. 11a). The *Te* values over the JFR (Fig. 11b) are lower than to the north (less than +20km), indicative of weakened oceanic crust over the ridge (Fig. 9). The minimum *Te* values in this area are well correlated with active volcanoes over the Nazca plate. Eastward, where the ridge does not present a 'topographic' signal, the plate becomes more rigid and then weakens again in the vicinity of the flexural bulge, where it reaches a constant value of *c.* 10 km (Fig. 11b).

East to the trench, the *Te* values rise up to *c.* +50 km. The velocity of growth for this region is greater in profile 2 than in profile 1, but once it reaches its maximum it decays abruptly in profile 2. The opposite occurs to the north (profile 1), where the transition is more subtle, reaching the maximum *Te* under the coastline. This value is maintained for a few kilometres to the east (Fig. 11a) and is characteristic of the flat-slab segments as exposed previously (Fig. 9). The rigidity then decays continuously to almost 0 km under the main Andes along both profiles.

The high topographic load of the main Andes is expressed by a minimum in the Bouguer anomaly, a minimum in the *Tzz* and a minimum in the Moho depths (Fig. 11). Based on the above we can say that the low values of *Te* in this section are related to the local compensation of the Andes root (Fig. 11). In profile 1, the *Te* values increases eastwards to the Precordillera, while in profile 2 the low *Te* values are maintained eastwards due to the presence of the asthenospheric wedge.

The SP exhibit distinct behaviour to the south and north. The Western SP exhibit intermediate *Te* values (more than 30 km), which then decay eastwards approaching the Eastern SP (profile 1). The behaviour to the south is rather distinct (profile 2). Once the *Te* values reach their minimum values they are maintained, except at the Cuyana Basin where they become more rigid. Low *Te* values are maintained over the southern ending of the SP. Shallower Moho depths and smaller *Te* values at the southern region of the SP indicate a weakened continental crust in this region compared to that in the north (Fig. 12). This region exhibits a low seismic activity (Fig. 10c). The opposite occurs in the northern region, where hypocentral seismicity (Fig. 10c) shows greater activity related to the JFR (as explained by Anderson *et al.* (2007), among others).

Conclusions

Deformation in the overriding plate, volcanism and discontinuities in the pattern of seismicity reflect anomalies through the Benioff zones that are caused by flat subduction. Previous work (e.g. Pérez-Gussinyé *et al.* (2008) has shown that subduction-related processes, as variations in the subduction angle, are related to variations in the compositional and thermal structure of the continental lithosphere modifying its flexural strength. The new global Earth gravity field models and exclusive satellite-only data offer a tool for studies on a regional scale, for example by determining the connections between anomalously thickened subducted oceanic crust (as is the case for the JFR) and the associated deformational effects in the overriding plate.

Calculation of the *Tzz* was performed with both EGM2008 and GOCE, allowing optimization with the higher resolution of EGM2008 (but reduced quality over the Andes) and the uniform quality of the GOCE data (but reduced spatial resolution). From these we delineated the main tectonic features, as intruded denser bodies in the region defined by 31°–34°S and 66–80°W. Then, using the Bouguer anomaly obtained from GOCE satellite data, we calculated the crustal and upper mantle discontinuity and the *Te* using the convolution approach. This method makes use of a newly derived analytical solution for the fourth-order differential equation that describes the flexure of a thin plate.

Downloaded from http://sp.lyellcollection.org/ by guest on March 10, 2015

The results obtained show a weakening of the oceanic plate over the track of the JFR and over the flexural bulge. We obtained substantial variations in the crustal structure of the continental lithosphere in the northern zone when compared to the south. To the north, where the flat slab occurs, plate rigidity is greater than in the southern zone where the oceanic plate subducts with an approximately normal angle. Here, the plate rigidity appears to be equivalent to zero, reflecting a weakened continental lithosphere due to the ascent of the magmas from the asthenophere. We obtained a gross correlation between the estimated *Te* values and some terranes, such as Precordillera, Cuyania, Famatina and Rio de la Plata Craton. Chilenia appears to be greatly affected by the differences in subduction angle, whereas the SP presents a distinct behaviour representing more rigidity in the northern region, and a weakened crust to the south and to the east. The results for *Te* indicate that the crustal structure in the region under study is far from homogeneous, with contrasting differences in strength properties.

The authors acknowledge the use of the GMT-mapping software of Wessel & Smith (1998). The authors also thank the Ministerio de Ciencia y Tecnica–Agencia de Promocion Cientıfica y Tecnologica, PICT07–1903, Agenzia Spaziale Italiana for the GOCE–Italy Project, the Ministero dell'Istruzione, dell'Universita' e della Ricerca (MIUR) under project PRIN, 2008CR4455_003 for financial support, and ESA for granting AO_GOCE_proposal_4323_Braitenberg.

Appendix I: Statistical analysis

We calculated the gravity anomaly derived from the EGM2008 model (Pavlis *et al.* 2008) and from the GOCE satellite (Pail *et al.* 2011) up to $N = 250$. The absolute value of the difference field (EGM2008-GOCE) is shown in Fig. A1. Statistical parameters for the difference between the two fields are shown in Table A1. A high-quality region is compared with a low-quality region in terms of the residual histogram. The white square in Fig. A1 marks a $1^\circ \times 1^\circ$ area with relatively high quality, which is compared to a square of equal size (black) of degraded quality. The histograms of the residuals (Fig. A2) illustrate the higher values for the black square.

The root-mean-square deviation was calculated from the mean on sliding windows measuring $0.5^\circ \times 0.5^\circ$ as a statistical measure of EGM2008 quality. The result is shown on Fig. A3. The most frequent value of the root-mean-square deviation is 3 mGal as shown in Fig. A4. The locations where the terrestrial data have problems reflects greatly increased values (up to −48 mGal).

The sparseness of terrestrial data in large regions, especially in areas of difficult access, and a non-unified height system used in different terrestrial studies resulted in these differences. The precision of the height measurements directly affects the accuracy of the (inland) gravity observations and their derivatives, and greater inconsistencies arise when considering large areas (Reguzzoni & Sampietro 2010). This highlights the usefulness of satellite-only derived data in mountainous areas that are difficult to access, as in the central to eastern region under study (see Braitenberg *et al.* (2011*a*, *b*) and Alvarez *et al.* (2012) for a more detailed explanation).

Table A1. *Statistical parameters for the difference*

Average difference	0.173 mGal
Standard deviation	15.208 mGal
Maximal value of difference	−48.109 mGal

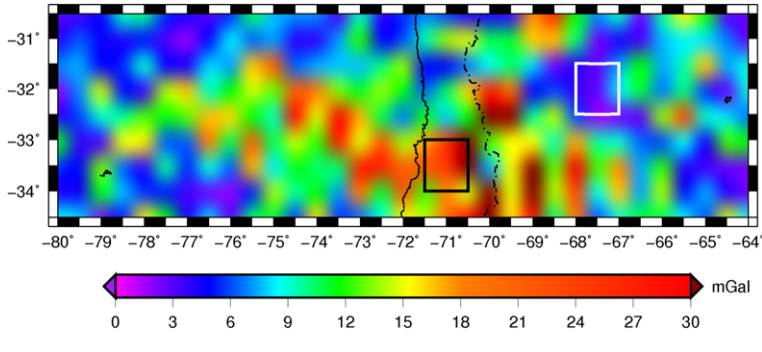

Fig. A1. Absolute difference between the gravity anomalies from EGM2008 and GOCE. The black square over the Andes indicates an area with erroneous data. The white square indicates an area over the Sierras Pampeanas with better data. The national border is given by a dotted and dashed line, and the coastal border by a solid line. Erroneous terrestrial data or lack of it in the EGM2008 model generates these differences between the two fields.

Downloaded from http://sp.lyellcollection.org/ by guest on March 10, 2015

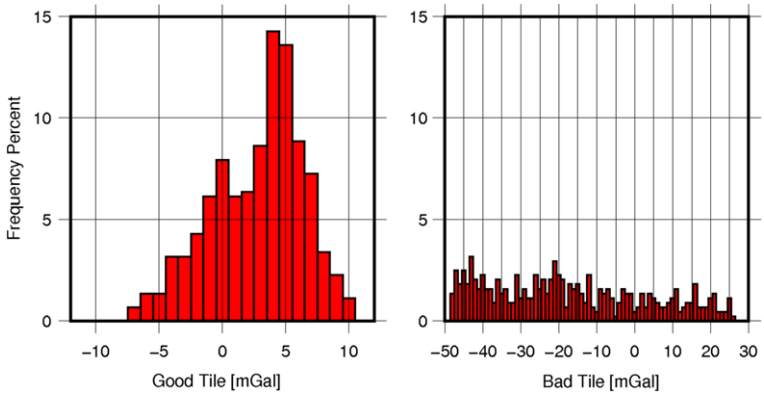

Fig. A2. Histogram of the residual gravity anomaly between EGM2008 and GOCE (up to degree and order $N = 250$). Left (good tile): white square of Figure A1. Right (bad tile): black square of Figure A1.

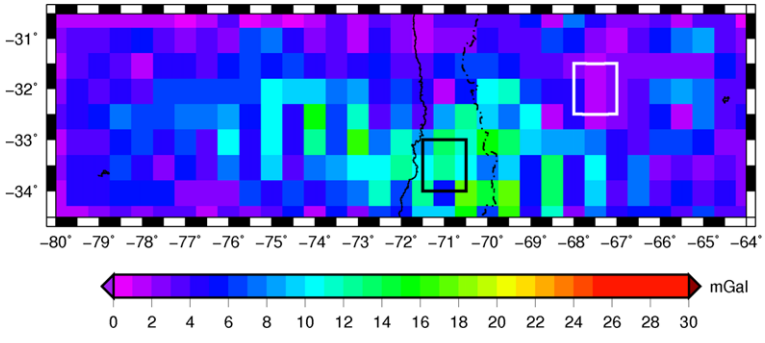

Fig. A3. Root mean square of the gravity anomaly residual on $0.5^\circ \times 0.5^\circ$ tiles.

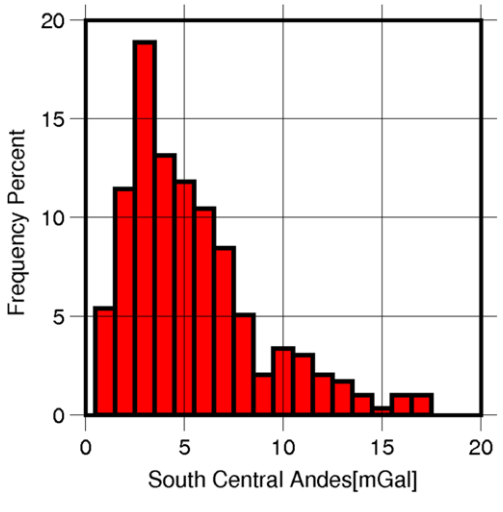

Fig. A4. Histogram of the root-mean-square deviations on $0.5^\circ \times 0.5^\circ$ tiles.

References

Allmendinger, R. W., Figueroa, D., Snyder, D., Beer, J., Mpodozis, C. & Isacks, B. L. 1990. Foreland shortening and crustal balancing in the Andes at 30°S Latitude. *Tectonics*, **9**, 789–809.

Allmendinger, R. W., Isacks, B. L., Jordan, T. E. & Kay, S. M. 1997. The evolution of the Altiplano–Puna plateau of the Central Andes. *Annual Review of the Earth and Planetary Science*, **25**, 139–174.

Alvarez, O., Gimenez, M. E., Braitenberg, C. & Folguera, A. 2012. GOCE satellite derived gravity and gravity gradient corrected for topographic effect in the South Central Andes region. *Geophysical Journal International*, **190**, 941–959, http://dx.doi.org/10.1111/j.1365-246X.2012.05556.x

Amante, C. & Eakins, B. W. 2009. *ETOPO1 1 Arc-Minute Global Relief Model: Procedures, Data Sources and Analysis*. National Oceanic and Atmospheric Administration Technical Memorandum NESDIS NGDC-24, 19 March 2009.

Anderson, M. L., Alvarado, P., Beck, S. & Zandt, G. 2007. Geometry and brittle deformation of the subducting Nazca plate, central Chile and Argentina. *Geophysical Journal International*, **171**, 419–434, http://dx.doi.org/10.1111/j.1365-246X.2007.03483.x

Downloaded from http://sp.lyellcollection.org/ by guest on March 10, 2015

ASTINI, R. A., MARTINA, F., EZPELETA, M., DÁVILA, F. M. & CAWOOD, P. A. 2009. Chronology from rifting to foreland basin in the Paganzo Basin (Argentina), and a reappraisal on the 'Eo- and Neohercynian' tectonics along Western Gondwana. *In*: *XII Congreso Geológico Chileno*, Santiago, 22–26 November 2009.

BANGS, N. L. & CANDE, S. C. 1997. Episodic development of a convergent margin inferred from structures and processes along the southern Chile margin. *Tectonics*, **16**, 489–505.

BARAZANGUI, M. & ISACKS, B. 1976. Spatial distribution of earthquakes and subduction of the Nazca Plate beneath South America. *Geology*, **4**, 686–692.

BARAZANGUI, M. & ISACKS, B. 1979. Subduction of the Nazca plate beneath Peru – evidence from spatial distribution of earthquakes. *Geophysical Journal of the Royal Astronomical Society*, **57**, 537–555.

BARREDO, S., CRISTALLINI, E., ZAMBRANO, O., PANDO, G. & GARCÍA, R. 2008. Análisis tectono-sedimentario del relleno de edad precuyana y cuyana inferior de la region del alto Kaufmann, Cuenca Neuquina. *In*: *VII Congreso de Exploración y Desarrollo de Hidrocarburos*, Mar del Plata, Argentina, November 2008, Actas, 443–446.

BARTHELMES, F. 2009. *Definition of Functionals of the Geopotential and their Calculation from Spherical Harmonic Models. Theory and formulas used by the calculation service of the International Centre for Global Earth Models (ICGEM)*. GFZ German Research Centre for Geosciences Scientific Technical Report **STR09/02**, http://icgem.gfz-postdam.de

BRAITENBERG, C. & DRIGO, R. 1997. A crustal model from gravity inversion in Karakorum. *In*: *International Symposium on Current Crustal Movement and Hazard Reduction in East Asia and South-East Asia*, Wuhan, 4–7 November, Symposium Procedures, 325–341.

BRAITENBERG, C. & ZADRO, M. 1999. Iterative 3D gravity inversion with integration of seismology data. Bollettino di Geophisica Teorica ed Applicata. *Proceedings of the 28th Joint Meeting IAG, Trieste, Italy*, **40**, 469–476.

BRAITENBERG, C., PETTENATI, F. & ZADRO, M. 1997. Spectral and classical methods in the evaluation of Moho undulations from gravity data: the NE Italian Alps and isostasy. *Journal of Geodynamics*, **23**, 5–22.

BRAITENBERG, C., EBBING, J. & GÖTZE, H. J. 2002. Inverse modelling of elastic thickness by convolution method – the Eastern Alps as a case example. *Earth Planetary Science Letters*, **202**, 387–404.

BRAITENBERG, C., WIENECKE, S. & WANG, Y. 2006. Basement structures from satellite-derived gravity field: South China Sea ridge. *Journal of Geophysical Research*, **111**, B05407, http://dx.doi.org/10.1029/2005JB003938

BRAITENBERG, C., WIENECKE, S., EBBING, J., BOM, W. & REDFIELD, T. 2007. Joint gravity and isostatic analysis for basement studies – a novel tool. *In*: *EGM 2007 International Wokshop, Innovation in EM, Grav and Mag Methods: A New Perspective for Exploration*, Villa Orlandi, Capri, Extended Abstracts.

BRAITENBERG, C., MARIANI, P., EBBING, J. & SPRLAK, M. 2011*a*. The enigmatic Chad lineament revisited with global gravity and gravity-gradient fields. *In*: VAN HINSBERGEN, D. J. J., BUITER, S. J. H., TORSVIK, T. H., GAINA, C. & WEBB, S. J. (eds) *The Formation and Evolution of Africa: A Synopsis of 3.8 Ga of Earth History*. Geological Society, London, Special Publications, **357**, 329–341, http://dx.doi.org/10.1144/SP357.18

BRAITENBERG, C., MARIANI, P. & PIVETTA, T. 2011*b*. GOCE observations in exploration geophysics. *In*: *Proceedings of 4th International GOCE User Workshop*, Munich, 31 March–1 April 2011, ESA SP-696.

BRATFISCH, R., JENTZSCH, G. & STEFFEN, H. 2010. A 3D Moho depth model for the Tien Shan from EGM2008 gravity data. *In*: *7th EGU General Assembly*, Vienna, 5 February 2010. Geophysical Research Abstracts 12, EGU2010-442. Poster presentation. Winner of the EGU Young Scientists Outstanding Poster Paper (YSOPP) Award 2010 in the Seismology division.

BROOKER, J. R., FAVETTO, A. & POMPOSIELLO, M. C. 2004. Low electrical resistivity associated with plunging of the Nazca flat slab beneath Argentina. *Nature*, **429**, 399–403.

BUROV, E. B. & DIAMENT, M. 1995. The effective elastic thickness (Te) of continental lithosphere: what does it really mean? *Journal of Geophysical Research*, **100**, 3905–3927.

CAHILL, T. & ISACKS, B. 1992. Seismicity and shape of the subducted Nazca plate. *Journal of Geophysical Research*, **97**, 17 503–17 529.

CONTRERAS-REYES, E. & OSSES, A. 2010. Lithospheric flexure modelling seaward of the Chile trench: implications for oceanic plate weakening in the Trench Outer Rise region. *Geophysical Journal International*, **182**, 97–112.

DAHLQUIST, J., ALASINO, P. H., EBY, N. E., GALINDO, C. & CASQUET, C. 2010. Fault controlled Carboniferous A-type magmatism in the proto-Andean foreland (Sierras Pampeanas, Argentina): geochemical constraints and petrogenesis. *Lithos*, **115**, 65–81.

DEMETS, C., GORDON, R. G. & ARGUS, D. F. 2010. Geologically current plate motions. *Geophysical Journal International*, **181**, 1–80, http://dx.doi.org/10.1111/j.1365-246X.2009.04491.x

DIVINS, D. L. 2003. *Total Sediment Thickness of the World's Oceans & Marginal Seas*. NOAA National Geophysical Data Center, Boulder.

EBBING, J., BRAITENBERG, C. & GÖTZE, H. J. 2001. Forward and inverse modeling of gravity revealing insights into crustal structures of the Eastern Alps. *Tectonophysics*, **337**, 191–208.

EBBING, J., BRAITENBERG, C. & WIENECKE, S. 2007. Insights into the lithospheric structure and tectonic setting of the Barents Sea region from isostatic considerations. *Geophysical Journal International*, **171**, 1390–1403.

EHB-CATALOG 2009. *International Seismological Centre EHB Bulletin*. International Seismological Center, Thatcham, http://www.isc.ac.uk

ENGDAHL, E. R., VAN DER HILST, R. & BULAND, R. 1998. Global teleseismic earthquake relocation with improved travel times and procedures for depth determination. *Bulletin of the Seismological Society of America*, **88**, 722–743.

FERNANDEZ SEVESO, F. & TANKARD, A. 1995. Tectonics and stratigraphy of the late Paleozoic Paganzo Basin

Downloaded from http://sp.lyellcollection.org/ by guest on March 10, 2015

of western Argentina and its regional implications. *In*: TANKARD, A. J., SUÁREZ SORUCO, R. & WELSINK, H. J. (eds) *Petroleum Basins of South America*. American Association of Petroleum Geologists, Tulsa, Memoirs, 285–301.

FERRACCIOLI, F., FINN, C. A., JORDAN, T. A., BELL, R. E., ANDERSON, L. M. & DAMASKE, D. 2011. East Antarctic rifting triggers uplift of the Gamburtsev Mountains. *Nature*, **479**, 388–392, http://dx.doi.org/10.1038/nature10566

FLOBERGHAGEN, R., FEHRINGER, M. *ET AL*. 2011. Mission design, operation and exploitation of the gravity field and steady-state ocean circulation explorer mission. *Journal of Geodesy*, **85**, 749–758.

GANS, C., BECK, S., ZANDT, G., GILBERT, H., ALVARADO, P., ANDERSON, M. & LINKIMER, L. 2011. Continental and oceanic crustal structure of the Pampean flat slab region, western Argentina, using receiver function analysis: new high-resolution results. *Geophysical Journal International*, **186**, 45–58.

GATTI, A., REGUZZONI, M. & VENUTI, G. 2013. The height datum problem and the role of satellite gravity models. *Journal of Geodesy*, **87**, 15–22. http://dx.doi.org/10.1007/s00190-012-0574-3

GIMENEZ, M. E., MARTÍNEZ, M. P. & INTROCASO, A. 2000. A Crustal Model based mainly on Gravity data in the Area between the Bermejo Basin and the Sierras de Valle Fértil–Argentina. *Journal of South American Earth Sciences*, **13**, 275–286.

GIMENEZ, M. E., BRAITENBERG, C., MARTINEZ, M. P. & INTROCASO, A. 2009. A comparative analysis of seismological and gravimetric crustal thicknesses below the Andean Region with flat subduction of the Nazca Plate. *Journal of Geophysics*, **2009**, 607458, http://dx.doi.org/10.1155/2009/607458

GOETZE, C. & EVANS, B. 1979. Stress and temperature in the bending lithosphere as constrained by experimental rock mechanism. *Geophysical Journal of the Royal Astronomical Society*, **59**, 463–478.

GUTSCHER, M. A. 2000. An Andean model of interplate coupling and strain partitioning applied to the flat subduction of SW Japan (Nankai Trough). *Tectonophysics*, **333**, 95–109.

GUTSCHER, M. A., SPAKMAN, W., BIJWAARD, H. & ENGDAHL, E. R. 2000. Geodynamics of flat subduction: seismicity and tomographic constraints from the Andean margin. *Tectonics*, **19**, 814–833.

HACKNEY, R. I., ECHTLER, H. P., FRANZ, G., GÖTZE, H. J., LUCASSEN, F., MARCHENKO, D., MELNICK, D., MEYER, U., SCHMIDT, S., TAŠÁROVÁ, Z., TASSARA, A. & WIENECKE, S. 2006. The segmented overriding plate and coupling at the south-central Chile margin (36–42°S). *In*: ONCKEN, O., CHONG, G., FRANZ, G., GIESE, P., RAMOS, V. A., STRECKER, M. R. & WIGGER, P. (eds) *The Andes: Active Subduction Orogen*. Springer Verlag, Berlin, Frontiers in Earth Sciences, **1**, 355–374.

INTROCASO, A., PACINO, M. C. & FRAGA, H. 1992. Gravity, isostasy and Andean crustal shortening between latitudes 30°S and 35°S. *Tectonophysics*, **205**, 31–48.

INTROCASO, A., PACINO, M. C. & GUSPI, F. 2000. The Andes of Argentina and Chile: crustal configuration, isostasy, shortening and tectonic features from gravity data. *Temas de Geociencia*, **5**, 31.

JAMES, D. E. & SACKS, S. 1999. Cenozoic formation of the Central Andes: a geophysical perspective. *In*: SKINNER, B. (ed) *Geology and Mineral Deposits of Central Andes*. Society of Economic Geology, London, Special Publications, **7**, 1–25.

JORDAN, T. E. & ALLMENDINGER, R. 1986. The Sierras Pampean of Argentina: a modern analogue of Rocky Mountain foreland deformation. *American Journal of Science*, **286**, 737–764.

JORDAN, T. E., ISACKS, B., ALLMENDINGER, R., BREWER, J., RAMOS, V. A. & ANDO, C. J. 1983*a*. Andean tectonics related to geometry of the subducted Nazca Plate. *Geological Society of America Bulletin*, **94**, 341–361.

JORDAN, T. E., ISACKS, B., RAMOS, V. A. & ALLMENDINGER, R. 1983*b*. Mountain building in the Central Andes. *Episodes*, **3**, 20–26.

KAY, S. M. & ABBRUZZI, J. M. 1996. Magmatic evidence for Neogene lithospheric evolution of the central Andean 'flat-slab' between 30°S and 32°S. *Tectonophysics*, **259**, 15–28.

KAY, S. M. & COIRA, B. 2009. Shallowing and steepening subduction zones, continental lithospheric loss, magmatism, and crustal flow under the Central Andean Altiplano–Puna Plateau. *In*: KAY, S., RAMOS, V. & DICKINSON, W. (eds) *Backbone of the Americas: Shallow Subduction Plateau Uplift and Ridge and Terrane Collision*. Geological Society of America, Boulder, Colorado, USA, Memoirs, **204**, 229–259.

KAY, S. M. & MPODOZIS, C. 2002. Magmatism as a probe to the Neogene shallowing of the Nazca plate beneath the modern Chilean flat-slab. *Journal of South American Earth Science*, **15**, 39–57.

KAY, S. M., MAKSAEV, V., MOSCOSO, R., MPODOZIS, C., NASI, C. & GORDILLO, C. E. 1988. Tertiary Andean magmatism in Chile and Argentina between 28 and 33°S: correlation of magmatic chemistry with a changing Benioff zone. *Journal of South American Earth Science*, **1**, 21–38.

KAY, S. M., MPODOZIS, C., RAMOS, V. A. & MUNIZAGA, F. 1991. Magma source variations for mid–late Tertiary magmatic rocks associated with a shallowing subduction zone and thickening crust in the Central Andes (28–33°S). *In*: HARMON, R. S. & RAPELA, C. W. (eds) *Andean Magmatism and Its Tectonic Setting*. Geological Society of America, Boulder, Colorado, USA, Special Papers, **26**, 113–137.

KAY, S. M., MPODOZIS, C. & COIRA, B. 1999. Neogene magmatism, tectonism and mineral deposits of the Central Andes (22°–33°S latitude). *In*: SKINNER, B. (ed) *Geology and Ore Deposits of the Central Andes*. Society of Economic Geology, London, Special Publications, **7**, 27–59.

KOKOGIAN, D. A., SEVESO, F. F. & MOSQUERA, A. 1993. Las secuencias sedimentarias triásicas. *In*: RAMOS, V. A. (ed.) *Geología y Recursos Naturales de Mendoza*. XII Congreso Geología Argentina y II Congreso de Exploración de Hidrocarburos, Relatorio, Mendoza, **I**, 65–78.

LOWRY, A. R., RIBE, N. M. & SMITH, R. B. 2000. Dynamic elevation of the Cordillera, western United States. *Journal of Geophysical Research*, **105**, 23371–23390.

LYON-CAEN, H. & MOLNAR, P. 1983. Constraints on the structure of the Himalaya from an analysis of gravity

Downloaded from http://sp.lyellcollection.org/ by guest on March 10, 2015

anomalies and a flexural model of the lithosphere. *Journal of Geophysical Research*, **88**, 8171–8191.

Martinod, J., Husson, L., Roperch, P., Guillaume, B. & Espurt, N. 2010. Horizontal subduction zones, convergence velocity and the building of the Andes. *Earth and Planetary Science Letters*, **299**, 299–309.

McGeary, S., Nur, A. & Ben-Avraham, Z. 1985. Spatial gaps in arc volcanism: the effect of collision or subduction of oceanic plateaus. *Tectonophysics*, **119**, 195–221.

Milana, J. P. & Alcober, O. 1994. Modelo tectosedimentario de la cuenca triásica de Ischigualasto (San Juan, Argentina). *Revista de la Asociación Geológica Argentina*, **49**, 217–235.

Miranda, S. & Robles, J. A. 2002. Posibilidades de atenuación cortical en la cuenca Cuyana a partir del análisis de datos de gravedad. *Revista de la Asociación Geológica Argentina*, **57**, 271–279.

Müller, R. D., Sdrolias, M., Gaina, C. & Roest, W. R. 2008. Age, spreading rates and spreading symmetry of the world's ocean crust. *Geochemistry Geophysics Geosystems*, **9**, Q04006, http://dx.doi.org/10.1029/2007GC001743

Oldenburg, D. 1974. The inversion and interpretation of gravity anomalies. *Geophysics*, **39**, 526–536.

Pail, R., Bruisma, S. *et al*. 2011. First GOCE gravity field models derived by three different approaches. *Journal of Geodesy*, **85**, 819–843.

Parker, R. L. 1972. The rapid calculation of potential anomalies. *Geophysical Journal of the Royal Astronomical Society*, **31**, 447–455.

Pavlis, N. K., Holmes, S. A., Kenyon, S. C. & Factor, J. K. 2008. An Earth Gravitational Model to degree 2160: EGM2008. Paper presented at the *2008 General Assembly of the European Geosciences Union*, Vienna.

Pavlis, N. K., Holmes, S. A., Kenyon, S. C. & Factor, J. K. 2012. The development and evaluation of the Earth Gravitational Model 2008. *Journal of Geophysical Research*, **117**, B04406.

Pérez-Gussinyé, M., Lowry, A. R., Watts, A. B. & Velicogna, I. 2004. On the recovery of the effective elastic thickness using spectral methods: examples from synthetic data and the Fennoscandian shield. *Journal of Geophysical Research*, **109**, 409.

Pérez-Gussinyé, M., Lowry, A. R., Phipps Morgan, J. & Tassara, A. 2008. Effective elastic thickness variations along the Andean margin and their relationship to subduction geometry. *Geochemistry Geophysics Geosystems*, **9**, Q02003.

Pilger, R. H. 1981. Plate reconstructions, aseismic ridges, and low-angle subduction beneath the Andes. *Geological Society of America Bulletin*, **92**, 448–456.

Ramos, V. A. 2009. Anatomy and global context of the Andes: main geologic features and the Andean orogenic cycle. *In*: Kay, S., Ramos, V. A. & Dickinson, W. (eds) *Backbone of the Americas: Shallow Subduction, Plateau Uplift, and Ridge and Terrane Collision*. Geological Society of America, Boulder, Colorado, USA, Memoirs, **204**, 31–65.

Ramos, V. A. & Folguera, A. 2009. Andean flat subduction through time. *In*: Murphy, B., Keppie, J. & Hynes, A. (eds) *Ancient Orogens and Modern Analogues*. Geological Society, London, Special Publications, **327**, 31–54.

Ramos, V. A., Munizaga, F. & Kay, S. M. 1991. El magmatismo cenozoico a los 33°S de latitud: Geocronologia y relaciones tectónicas. Paper presented at *6° Congreso Geológico Chileno*, Viña del Mar, Chile, Actas, **1**, 892–896.

Ramos, V. A., Cristallini, E. O. & Perez, D. 2002. The Pampean flat-slab of the Central Andes. *Journal of South American Earth Science*, **15**, 59–78.

Ramos, V. A., Vujovich, G., Martino, R. & Otamendi, J. 2010. Pampia: a large cratonic block missing in the Rodinia supercontinent. *Journal of Geodynamics*, **50**, 243–255.

Ranero, C., von Huene, R., Weinrebe, W. & Reichert, C. 2006. Tectonic processes along the Chile convergent margin. *In*: Oncken, O., Chong, G. *et al*. (eds) *The Andes, Active Subduction Orogeny*. Springer-Verlag, Berlin/Heidelberg/New York, Frontiers in Earth Science Series, 91–121.

Reguzzoni, M. & Sampietro, D. 2010. An inverse gravimetric problem with GOCE data. *International Association of Geodesy Symposia, 'Gravity, Geoid and Earth Observation'*, **135**, 451–456, http://dx.doi.org/10.1007/978-3-642-10634-7_60

Rossello, E. A., Limarino, C. O., Ortiz, A. & Hernández, N. 2005. Cuencas de los Bolsones de San Juan y La Rioja. *In*: Chebili, G., Cortiñas, J. S., Spalletti, L. A., Legarreta, L. & Vallejo, E. L. (eds) *Simposio Frontera Exploratoria de la Argentina*. VI Congreso de Exploración y Desarrollo de Hidrocarburos, Mar del Plata, Argentina, 147–173.

Sacek, V. & Ussami, N. 2009. Reappraisal of the effective elastic thickness for the sub-Andes using 3-D finite element fexural modelling, gravity and geological constraints. *Geophysical Journal International*, **179**, 778–786.

Sacks, I. S. 1983. The subduction of young lithosphere. *Journal of Geophysical Research*, **88**, 3355–3366.

Sandwell, D. T. & Smith, W. H. F. 1997. Marine gravity anomaly from Geosat and ERS-1 satellite altimetry. *Journal of Geophysical Research*, **102**, 10 039–10 050.

Siebert, L. & Simkin, T. 2002. *Volcanoes of the World: An Illustrated Catalog of Holocene Volcanoes and Their Eruptions*. Smithsonian Institution, Washington DC, USA, Global Volcanism Program Digital Information Series, GVP-3, http://www.volcano.si.edu/world/

Smalley, R. & Isacks, B. 1987. A high resolution local network study of the Nazca Plate Wadati–Benioff Zone under Western Argentina. *Journal of Geophysical Research*, **92**, 13903–13912.

Stauder, W. 1973. Mechanism and spatial distribution of Chilean earthquakes with relation to subduction of the oceanic plate. *Journal of Geophysical Research*, **78**, 5033–5061.

Steffen, R., Steffen, H. & Jentzsch, G. 2011. A three-dimensional Moho depth model for the Tien Shan from EGM2008 gravity data. *Tectonics*, **30**, TC5019, http://dx.doi.org/10.1029/2011TC002886

Stewart, J. & Watts, A. B. 1997. Gravity anomalies and spatial variations of flexural rigidity at mountain ranges. *Journal of Geophysical Research*, **102**, 5327–5352.

Tassara, A. 2005. Interaction between the Nazca and South American plates and formation of the Altiplano–Puna

Downloaded from http://sp.lyellcollection.org/ by guest on March 10, 2015

plateau: review of a flexural analysis along the Andean margin (15°–34°S). *Tectonophysics*, **399**, 39–57.

Tassara, A. & Yañez, G. 2003. Relación entre el espesor elástico de la litósfera y la segmentación tectónica del margen Andino (15–478S). *Revista Geológica de Chile*, **30**, 159–186.

Tassara, A., Swain, C., Hackney, R. & Kirby, J. 2007. Elastic thickness structure of South America estimated using wavelets and satellite-derived gravity data. *Earth and Planetary Science Letters*, **253**, 17–36.

Tebbens, S. F. & Cande, S. C. 1997. Southeast Pacific tectonic evolution from early Oligocene to present. *Journal of Geophysical Research*, **102**, 12 061–12 084.

Uieda, L., Ussami, N. & Braitenberg, C. F. 2010. Computation of the gravity gradient tensor due to topographic masses using tesseroids. *EOS, Transactions AGU*, **91** Meeting of the Americas Supplement, Abstract G22A-04, http://leouieda.github.io/tesseroids/

von Huene, R., Corvalán, J., Flueh, E. R., Hinz, K., Korstgard, J., Ranero, C. R., Weinrebe, W. & CONDOR SCIENTISTS 1997. Tectonic control of the subducting Juan Fernández Ridge on the Andean margin near Valparaiso, Chile. *Tectonics*, **16**, 474–488.

Watts, A. 2001. *Isostasy and Flexure of the Lithosphere*. Cambridge University Press, Cambridge, UK.

Weidmann, C., Spagnotto, S., Gimenez, M. E., Martinez, P., Álvarez, O., Sanchez, M. & Linceklinger, F. 2013. Crustal structure and tectonic setting of the south central Andes from gravimetric analysis. *Geofisica Internacional*, **52**, 121–133.

Wessel, P. & Smith, W. H. F. 1998. New, improved version of the generic mapping tools released. *EOS, Transactions of the American Geophysical Union*, **79**, 579.

Wienecke, S. 2002. *Homogenisierung und Interpretation des Schwerefeldesentlang der SALTTraversézwischen 36°–42°S*. Unpublished diploma thesis, FreieUniversität, Berlin.

Wienecke, S. 2006. *A new analytical solution for the calculation of flexural rigidity: significance and applications*. PhD thesis, Free University Berlin, http://www.diss.fu-berlin.de/2006/42

Wienecke, S., Braitenberg, C. & Göetze, H. J. 2007. A new analytical solution estimating the flexural rigidity in the Central Andes. *Geophysics Journal International*, **169**, 789–794.

Yañez, G. & Cembrano, J. 2004. Role of viscous plate coupling in thelate Tertiary Andean tectonics. *Journal of Geophysical Research*, **109**, http://dx.doi.org/10.1029/2003JB002494

Yañez, G. A., Ranero, C. R., von Huene, R. & Diaz, J. 2001. Magnetic anomaly interpretation across the southern Central Andes (32°–34° S): the role of the Juan Fernandez Ridge in the late Tertiary evolution of the margin. *Journal of Geophysical Research, Solid Earth*, **106**, 6325–6345.

Zadro, M. & Braitenberg, C. 1997. Spectral methods in gravity inversion: the geopotential field and its derivatives. *Annali di geofisica XL*, **5**, 1433–1443.